On the mechanism of Sn tunnelling induced intermetallic formation between Sn-8Zn-3Bi solder alloys and Cu substrates

On the mechanism of Sn tunnelling induced intermetallic formation between Sn-8Zn-3Bi-xSb lead-free solder alloys and Cu substrates

Guang Ren* and Maurice N. Collins*

Stokes Laboratories, Bernal Institute, University of Limerick, Ireland.

*Corresponding author: Mr. Guang Ren (Guang.ren@ul.ie) Dr. Maurice N Collins (Maurice.collins@ul.ie) tel 353 61202867

Abstract

The interfacial reaction of Sn-8Zn-3Bi-xSb (x = 0, 0.5, 1.0, 1.5) on Cu substrate has been investigated under 150 °C thermal aging up to 720 h and an interfacial reaction mechanism, which governs the aging process, has been proposed. A 1 μm thin layer of scallop-shaped ε-$CuZn_5$ intermetallic compounds (IMCs) and a 4 μm thin layer of planar γ-Cu_5Zn_8 IMCs were formed at the interface after solder reflow. During initial aging, ε-$CuZn_5$ transformed to γ-Cu_5Zn_8 and the intermetallic layer (IML) at the interface thickened. As aging prolonged, Cu_5Zn_8 started to degrade due to the depletion of Zn and voids formed throughout the IML. These voids were rapidly filled by diffusing Sn atoms, inducing a tunnelling effect, allowing Sn to reach the Cu substrate and form Cu_6Sn_5 IMCs at the interface. The thickening of the IML is controlled by a diffusion mechanism and this is suppressed by introducing Sb as a micro-alloying component, hypothetically though the pinning effect to reduce the diffusion rate of Zn in Sn matrix.

Keywords

Solder; Interfacial reaction; Intermetallics; SnZnBi alloys; Micro alloying.

Introduction

Sn-Pb solder alloy has been used in the electronics industry for decades due to their low cost, good solderability and mechanical performance. However, Pb is toxic to both human health and environment and it was therefore banned by EU legislation (restriction on hazardous substances - RoHS) in 2006. Since then Sn-Ag-Cu (SAC) based alloys have been the interconnect materials of choice [1-3]. However, SAC based solder alloys have the following disadvantages: 1) the higher melting temperature up to 217 °C (compared to 183 °C of eutectic Sn-37Pb) limits their use with thermal sensitive components which are essential in aeronautical, medical and military applications; 2) the cost is higher due to the Ag; 3) higher processing temperature contradicts the global efforts to curb the carbon footprint; 4) coarsening of Ag_3Sn IMCs can induce brittle fracture at the interface and provide crack initiation sites, which result in reliability issues 5) resistance to drop impact and fatigue varies depended on Ag content difference, all of these makes it difficult to become a “drop-in” lead-free alterative of conventional eutectic Sn-37Pb solder alloy [4-11].

Sn-Zn based alloys have received increasing attention due to their low cost and more importantly, their low melting temperature, e.g., eutectic Sn-9Zn has a melting temperature of 198 °C, and shows comparable mechanical properties with Sn-37Pb [12]. Although highly-active Zn’s tendency to oxidise and react with flux mediums can result in poor wettability and shorter paste shelf life, this can be resolved by the development in micro-alloying [13] and flux technology [14]. Convinced by its potential to become the next generation low temperature lead-free replacement, numerous academia and industrial research teams have been actively researching Sn-Zn based solder alloys [15-22] and the latest findings have been reviewed [23]. Among these studies, Sn-8Zn-3Bi shows significantly improved wettability and mechanical properties, with an even lower melting temperature of 187 °C [24].

Most electronic device reliability issues are caused by solder joint failure rather than device malfunction. IMCs formed at the interface between solder alloy and substrate play a crucial role on maintaining a robust bond, both mechanically and electrically. However, the IML can become thicker at elevated temperature during normal use and becomes unstable due to IMCs' brittleness, which leads to crack formation, propagation and eventual failure [11, 25]. Hence, a full understanding of the mechanism governing the interfacial reaction is of vital importance to elucidate solder joint reliability.

At the interface, Cu is the most commonly used metallisation finish in electronic assemblies. Instead of Cu-Sn IMCs that form at SAC based solder/Cu interfaces, Cu-Zn IMCs are observed at Sn-Zn based solder/Cu interfaces. The initial interface is made up of a thin scalloped $CuZn_5$ layer adjacent to solder and a thick flat Cu_5Zn_8 adjacent to the Cu [22], but with longer reaction time $CuZn_5$ IMC transforms to Cu_5Zn_8 IMC [26, 27]. While Cu_5Zn_8 is the dominant reaction product at the as-soldered interface, Cu-Sn phases emerge at Cu_5Zn_8/Cu interface after long-term aging and have the tendency to replace the Cu-Zn phase [28-31]. In addition, some micro-alloys, such as Cu, Ni, Ag and Pr, were found to effectively supress the thickening of IML but simultaneously introduce extra IMCs or even induce Sn whiskers, both of which have a negative effect on reliability [19, 26, 27]

In a previous study, the authors of this paper found trace Sb alloying in Sn-8Zn-3Bi solder alloy can refine the microstructure without forming new IMCs and it enhanced mechanical properties through solid solution strengthening [32]. In this study, the long-term interfacial reaction of Sn-8Zn-3Bi-xSb/Cu during thermal aging at 150 °C has been investigated. The effect of Sb micro-alloying on IML growth has been discussed and an interfacial reaction mechanism has been proposed for these alloys, in order to predict and fully explain the microstructural evolution of Sn-8Zn-3Bi-xSb/Cu interface under isothermal aging.

Materials and experimental methods

Alloy powders consisting of Sn-8Zn-3Bi-xSb were purchased from 5N plus (Montreal, Canada). The Sb content in the Sn-8Zn-3Bi-xSb solder is 0, 0.5, 1.0 and 1.5 wt.%. A series of alloy ingots have been prepared from these alloy powders. Table 1 shows the final chemical composition of the alloy ingots, determined by inductively coupled plasma mass spectrometry (ICP-MS).

Table 1 The chemical composition of the solder alloys

Nominal composition (wt.%)	Final chemical composition (wt.%)			
	Sn	Zn	Bi	Sb
Sn-8Zn-3Bi	Balance	7.62	3.09	0
Sn-8Zn-3Bi-0.5Sb	Balance	7.39	3.01	0.52
Sn-8Zn-3Bi-1.0Sb	Balance	7.31	2.97	0.96
Sn-8Zn-3Bi-1.5Sb	Balance	7.27	2.97	1.44

The alloy ingot was machined into pieces, which were then punched to 0.3 g discs. Cu substrates (20 mm × 20 mm × 0.5 mm) have been ground to remove the surface oxides and ultrasonically cleaned in isopropyl alcohol (IPA). The alloy disc was then cleaned and placed on the Cu substrates, with flux coated, as shown in Figure 1. The solder/Cu coupon was placed in an oven at 250 °C for 3 min to conduct the reflow reaction. The spreading area and contact angle of each sample was measured using microscope and image analysis (ImageJ).

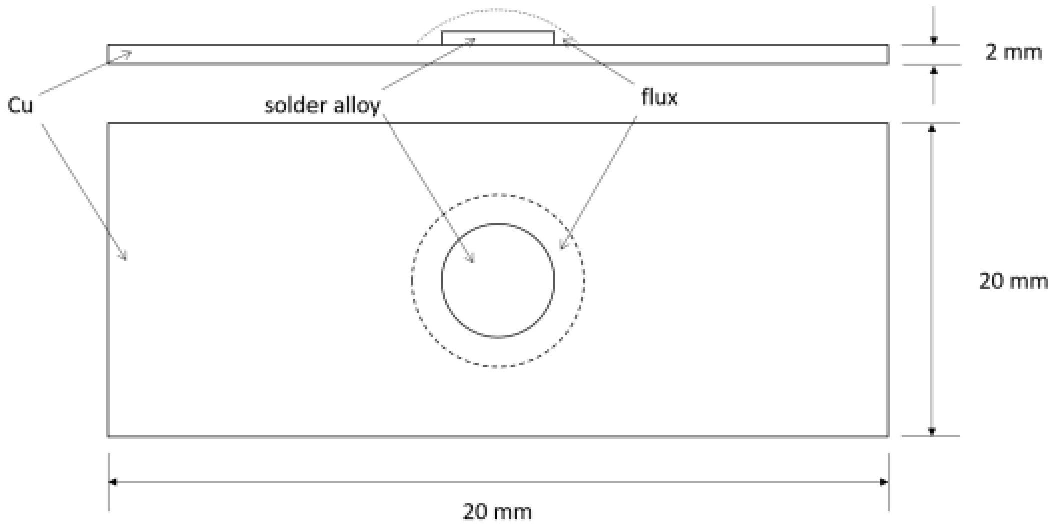

Figure 1 Diagram for solder/Cu coupon (not in scale)

Then the solder/Cu coupon was aged in an oven at 150 °C for: 72, 168, 240, 360 and 720 h respectively. An as-reflowed sample was left as a control. After aging, the sample was cross-sectioned and metallographically polished to 1 μm finish to reveal solder/Cu interface. Scanning electron microscope SEM (Hitachi SU70) and electron probe microanalysis (EPMA) were used to investigate the interfacial morphology. Energy dispersive spectrometer (EDS) was utilised to examine the composition of precipitated IMCs. The thickness of IML was measured from high magnification image using image analysis software ImageJ. As the thickness of IML varies along the interface, the thickness was measured by dividing the area of IML by its length along the interface. For each sample, at least 5 random locations were chosen along the interface and the average value was used as the representative thickness.

Results and discussion

Interfacial reactions between the Sn-8Zn-3Bi-xSb solder and the Cu substrate during reflowing

As a similar interfacial evolution process was observed for all four Sn-8Zn-3Bi-xSb/Cu coupons in this study, the Sn-8Zn-3Bi-1.5Sb/Cu coupon was selected as an example to elaborate the interfacial evolution. Figure 2 shows the SEM images of as-reflowed Sn-8Zn-3Bi-1.5Sb/Cu interfaces. Two IMLs can be found at the Sn-8Zn-3Bi-1.5Sb/Cu interface after reflowing, a 1 μm thick scallop-shaped layer adjacent to the solder alloy and a 4 μm thick planar layer next to the Cu substrate. From the EDS analysis result, the composition of scallop-shaped IMC (Spectrum 2) is 20 at. % Cu + 80 at. % Zn, which is confirmed as ε-$CuZn_5$. The composition of thicker planar IMC (Spectrum 1) is 37 at. % Cu + 63 at. % Zn, which is identified as γ-Cu_5Zn_8. Similar observations have been reported in numerous studies [26-29, 33]. The addition of Sb did not alter the as-reflowed interfacial morphology.

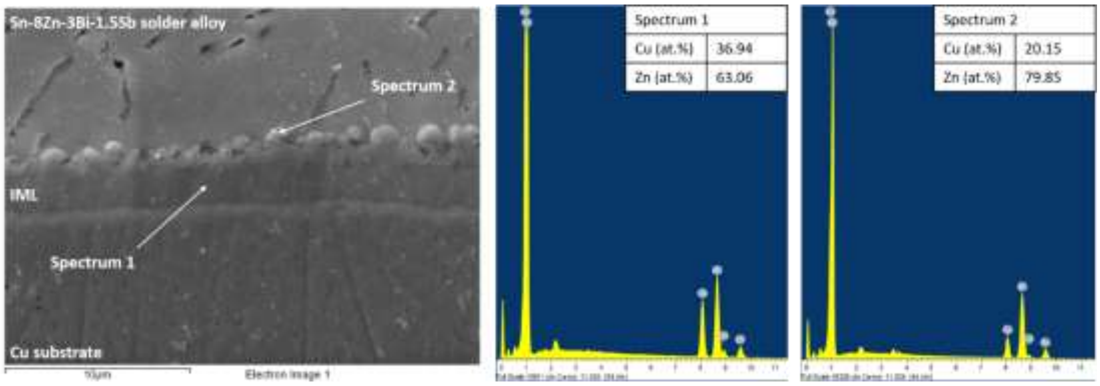

Figure 2 High magnification image of Sn-8Zn-3Bi-1.5Sb/Cu interface, with elemental composition analysed by EDS

Figure 3 shows the SEM morphology and the corresponding EDX line scan profiles from point A to B of the as-received interface of Sn-8Zn-3Bi-1.5Sb/Cu coupon soldered at 250 °C for 3 mins. The EDX line scan profile clearly confirmed the existence of the two layers of IMCs. The line scan profile across solder/Cu also revealed that Sb content decreases from the interface where IML forms, indicating that Sb did not participate in the interfacial reaction.

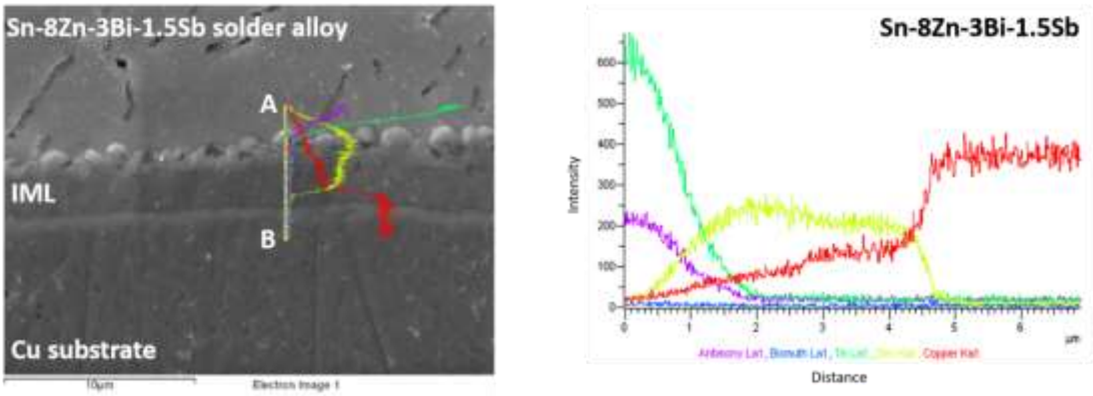

Figure 3 EDS line scan profile of Sn-8Zn-3Bi-1.5Sb/Cu interface

Figure 4 shows the elemental mapping analysis of the interface of Sn-8Zn-3B-1.5Sb/Cu after soldering at 250 °C for 3 min. It can be observed that the interfacial layer is mainly made up of Cu and Zn elements. Zn was primarily concentrated at the interfacial layers. The micro alloy Sb was homogeneously dissolved in the Sn. The granular Bi-rich phase commonly seen in Sn-8Zn-3Bi-based solder alloy bulk has not been detected near the solder/Cu interface.

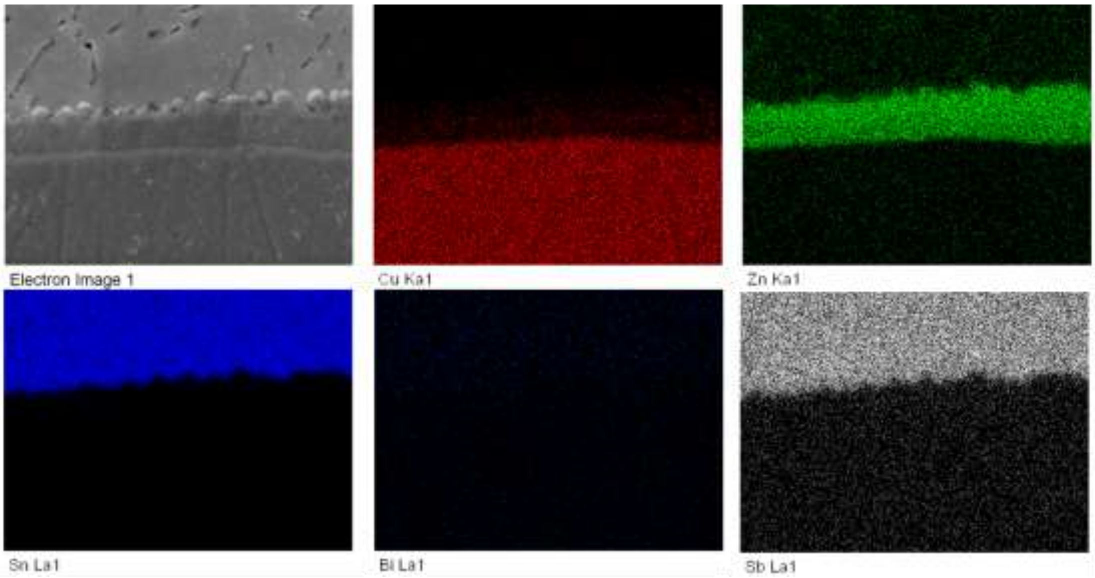

Figure 4 SEM morphology and EPMA mapping analysis of as-soldered Sn-8Zn-3Bi-1.5Sb/Cu interface

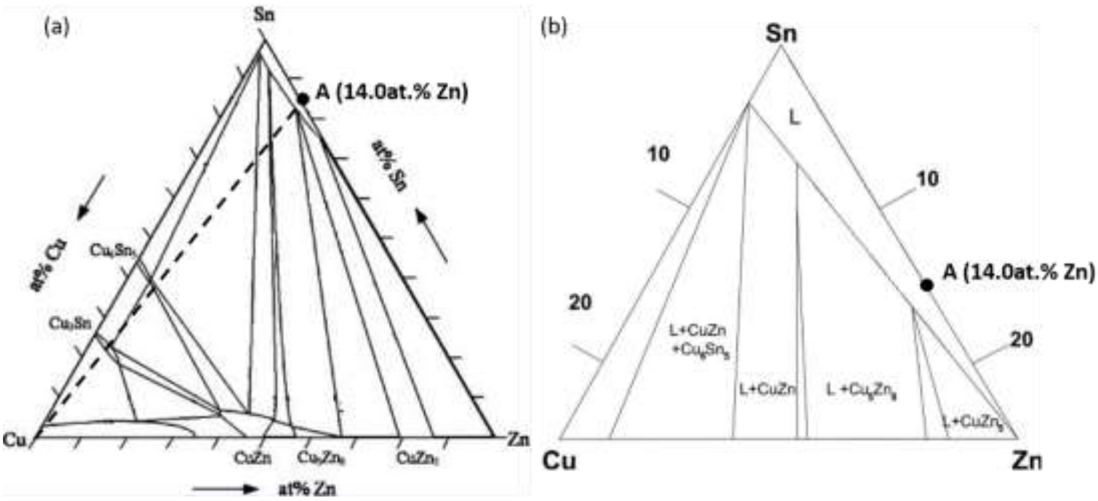

Figure 5 Isothermal section of Cu-Sn-Zn ternary phased diagram at 250 °C: (a) full-scale, (b) Sn-rich corner (redrawn from [34])

The local equilibrium at the reaction interfaces is an important assumption for interfacial reaction elucidation when governed by diffusion [35]. This assumes that the reaction products at the interface can be preliminarily predicted using phase diagrams [36]. Figure 5 represents the isothermal section of the ternary Cu-Sn-Zn phase diagram at 250 °C. Since the content of Zn in Sn-8Zn-3Bi-xSb solder is 14.0 at.%, the composition is represented by point “A” on the Sn-Zn baseline. If a line is drawn to connect point “A” and the Cu apex, it cuts right across the three-phase junction point of γ-Cu_5Zn_8/ε-$CuZn_5$/liquid. The driving force of flat γ-Cu_5Zn_8 formation is larger than that of scallop-shaped ε-$CuZn_5$ formation, based on a thermodynamic modelling [33]. Therefore, γ-Cu_5Zn_8 phase is the predominantly formed IMC at the Sn-8Zn-3Bi-xSb/Cu interface.

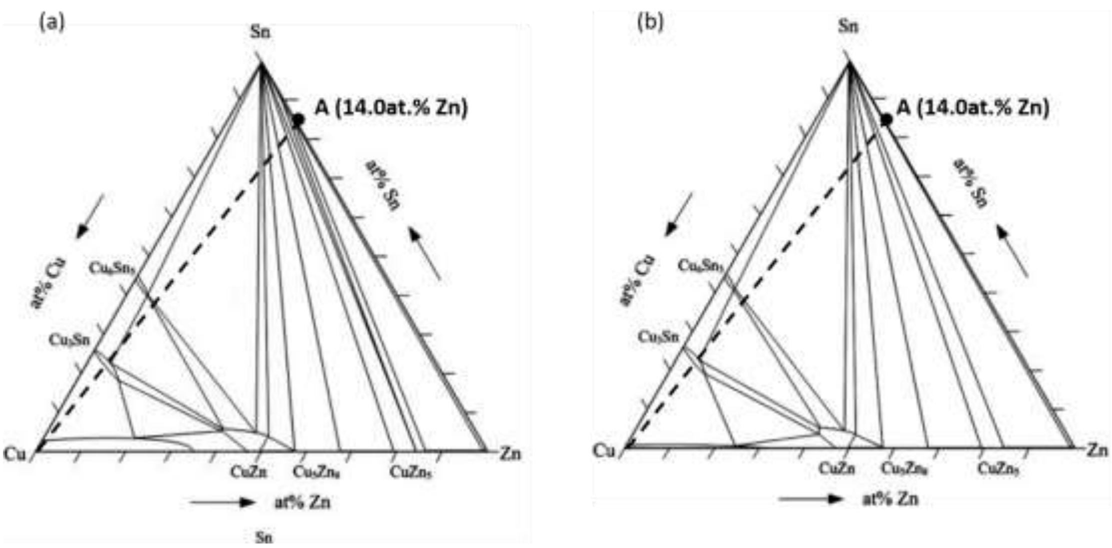

Figure 6 Isothermal Cu-Sn-Zn ternary phased diagram at (a) 210 °C and (b) 180 °C (redrawn from [34])

However, ε-$CuZn_5$ could also form through two subsequent peritectic reactions, i.e., L + γ-Cu_5Zn_8 → δ-$CuZn_3$ and L + γ-$CuZn_3$ → ε-$CuZn_5$ [37]. Figure 6 indicates that the intersection point of ε-$CuZn_5$ phase boundary at Sn-Zn baseline shifts towards the Sn apex as the temperature decreases. This indicates there is still strong possibility of ε-

CuZn5 formation during the cooling process after reflow. Experimental results reveal that both phases, ε-$CuZn_5$ and γ-Cu_5Zn_8, are formed at the as-reflowed interface, which is in well agreement of the thermodynamic prediction discussed above.

The dashed line connecting "A" point and Cu apex in Figure 5a also cuts across multiple phase boundaries and phase regions, including Cu_6Sn_5 and Cu_3Sn, which are both thermodynamically stable phases. However, Sn remained in the bulk solder alloy and did not form any Cu-Sn IMC with Cu at all solder/Cu interfaces, as clearly shown in Figure 3 and Figure 4. The absence of the Cu-Sn phases may be due to the limit of higher energy barrier of nucleation. Firstly, the Gibbs free energy of Cu-Zn IMCs formation is lower than that of Cu-Sn IMCs formation [38], this makes the Cu-Sn phases difficult to form. Therefore, when Cu atoms diffuse from the substrate towards the interface, they will preferentially react with the active Zn to form Cu-Zn IMCs, rather than to form Cu-Sn IMCs with Sn, at the Cu-8Zn-3Bi-xSb/Cu interface. Secondly, Cu-Sn phases may form but have a relatively slow growth rate, which makes them too thin to be observed microscopically. Based on the phase diagram of Cu-Sn-Zn, Cu-Sn phases should only form at the γ-Cu_5Zn_8/Cu interface, which in turn demands the diffusion of Sn from the solder alloy to the Cu substrate. However, since the Sn diffusion is retarded by the increasingly thicker Cu-Zn phases [28], formation of the Cu-Sn phases is expected to be increasingly unfavourable.

Interfacial evolutions between the Sn-8Zn-3Bi-xSb solder and the Cu substrate under aging

Figure 7 shows SEM morphology of the interface between Sn-8Zn-3Bi-1.5Sb and Cu substrate, with increasing aging time. It is shown that upon aging at 72 h, the scallop-shaped ε-$CuZn_5$ vanishes and the planar γ-Cu_5Zn_8 is the only IML at the interface which becomes thicker on aging, from 4 μm to 9 μm. The jagged features of the solder/IML interface may indicate the coalescence and transformation of ε-$CuZn_5$ IMC to γ-Cu_5Zn_8. Date et al. compared the diffusivity of each element in the case of eutectic-Sn/Zn/Cu and point out that Cu is the dominant diffusing species due to its highest diffusivity [39]. The diffusion speed of Cu atoms in Sn is approximately 1000~10,000 times larger than that of Zn atoms in Sn matrix [40, 41]. Due to lower diffusivity of Zn, the supply of Zn from the solder is insufficient for ε-$CuZn_5$ growth. On the other hand, ceaseless diffusion of Cu from Cu substrate rapidly complements the interfacial reaction, boosting the transformation of ε-$CuZn_5$ to γ-Cu_5Zn_8 phase.

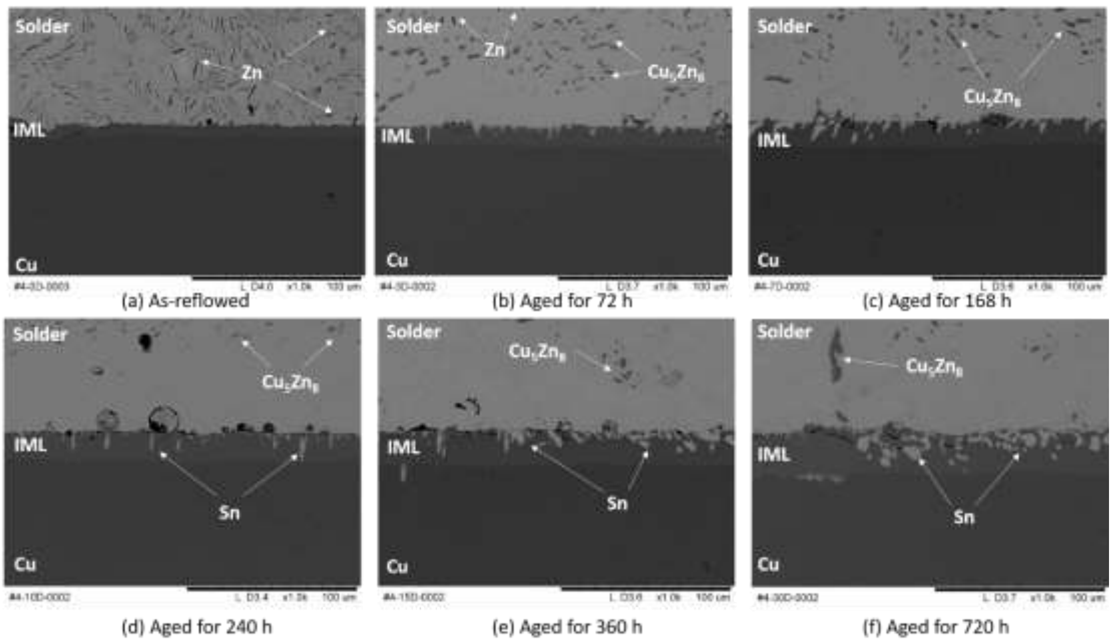

Figure 7 Sn-8Zn-3Bi-1.5Sb/Cu interfacial layer development with prolonged aging: (a) as-reflowed, (b) aged for 72 h, (c) aged for 168 h, (d) aged for 240 h, (e) aged for 360 h, (f) aged for 720 h

In addition, the standard Gibbs free energy of ε-$CuZn_5$ IMC formation is higher compared with that of γ-Cu_5Zn_8 IMC formation [42]. Thus, from the perspective of Gibbs free energy of formation and onset temperature of crystallisation, scallop-shaped ε-$CuZn_5$ will tend to transform to planar γ-Cu_5Zn_8 which is more thermodynamically stable. As a result, when the interfacial reaction time is long enough, e.g., aging at 150 ℃ for 72 h, the ε-$CuZn_5$ layer completely disappears and γ-Cu_5Zn_8 layer thickens.

Additionally, the number of needle-like primary Zn-rich phases at the solder side near the interface decreases and instead, some isolated γ-Cu_5Zn_8 particles were observed near the solder interface. This implies that some Cu atoms moved through the planar γ-Cu_5Zn_8 IML and reacted with the Zn atoms within the solder bulk to form isolated γ-Cu_5Zn_8 IMCs during aging, which can be ascribed to the larger magnitude of Cu diffusivity in Sn matrix compared to that of Zn.

The IML kept growing and became thicker as the aging time is prolonged, and this is shown in Figure 7a-f, Zn-rich phases in the solder matrix gradually disappeared due to the diffusion of Zn towards the joint interface. At the same time more isolated γ-Cu_5Zn_8 particles were formed in the solder matrix due to the rapid diffusion of Cu. Upon aging of 240 h, as shown in Figure 7d, no primary Zn-rich phases and very few γ-Cu_5Zn_8 particles can be found in the solder matrix near the interface. The growth of γ-Cu_5Zn_8 IML becomes slower with extended aging time and its morphology is serrated and discontinuous. After aging for 360 h, as shown in Figure 7e and f, a new phase emerged between the IML and the Cu substrate. This newly formed phase was identified as Cu_6Sn_5 IMC, as shown in Figure 8.

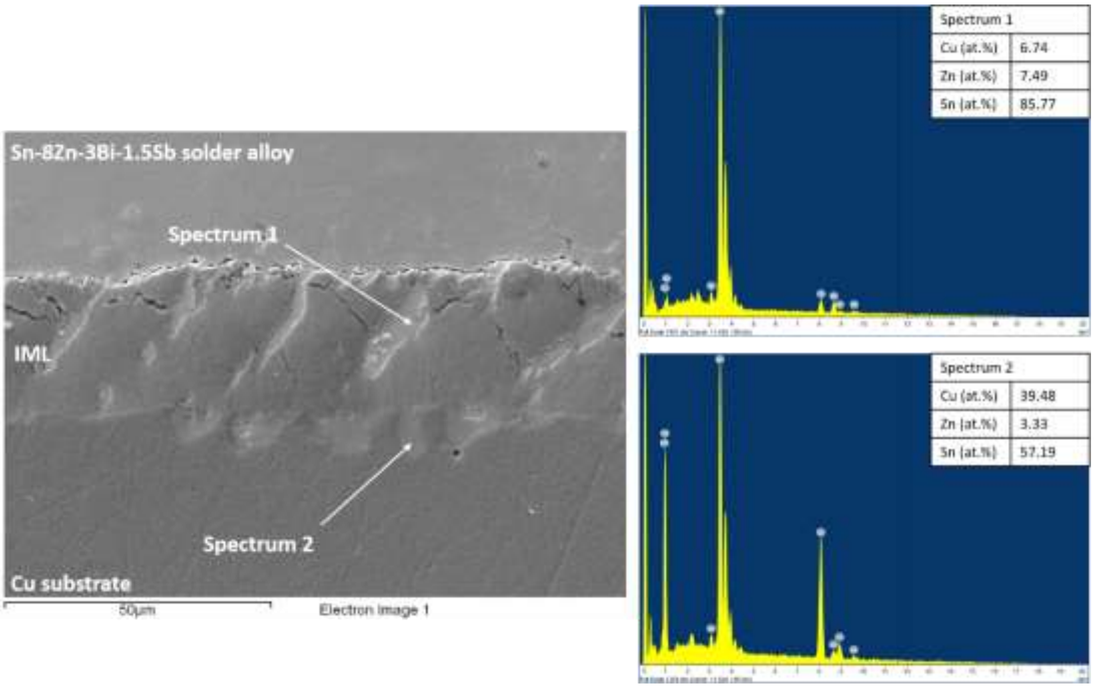

Figure 8 High magnification image of Sn-8Zn-3Bi-1.5Sb/Cu interface after 720 h of aging, with elemental composition analysed by EDS

Suganami et al. reported that the Cu–Zn IML of Sn-9Zn/Cu coupon was not stable at 150 °C and became thin. When the gap at the reaction layer was open, Sn directly reacts with the Cu substrate to form a Sn–Cu IMC growing deep into the substrate [43]. Duan el al. studied Sn-8Zn-3Bi/Cu interfacial reaction and reported the decomposition of the Cu-Zn IML by the diffusion of Zn into the Cu substrate. It was found that upon aging at 170 °C for 500 h three IMLs were detected at the interface: Cu-Zn IML in the middle of the reaction layers and Cu-Sn IMLs adjacent to it on both sides. Moreover, with increasing aging time to 1000 h the thickness of Cu-Zn IML decreased, while both the two Cu-Sn IMLs thickened at the same time. It was then concluded that the Cu-Zn IML acts as the diffusion channel for Cu and Sn just like a bridge [31].

Incorporating the observations from this study and hypothesis of Suganami et al. and Duan el al. introduced above. It can be assumed that during initial aging, the supply of diffusing Zn is sufficient and the γ-Cu_5Zn_8 IML grows accordingly and this acts as interfacial diffusion barrier that Sn atoms cannot penetrate through in order to react with Cu. However, as aging proceeds, the thickening of γ-Cu_5Zn_8 IML slows down as the Zn-rich phase from solder side depletes. The interfacial equilibrium then shifts due to inadequate Zn supply. As a result, the γ-Cu_5Zn_8 IMC becomes unstable and begins to degrade, leaving voids which are rapidly filled by Sn atoms diffusing (tunnelling) from the solder alloy. This also explains the serrated morphology of IML observed in Figure 7. This interfacial evolution continues with prolonged aging time, and Sn atoms continue to diffuse towards the Cu substrate, as can be clearly seen from elemental mapping in Figure 9, resulting in the ultimate formation of Cu_6Sn_5 IMCs at the interface, as shown in Figure 7e and f. However, it seems that Cu_6Sn_5 IMCs appear not only under the Sn channels, but also randomly between Cu_5Zn_8 and Cu substrate, as revealed in Figure 8. This is probably due to the metallurgical polishing's "wiping off" certain Sn tunnels which existed previously and lead to the formation of these seemingly randomly located Cu_6Sn_5 IMCs.

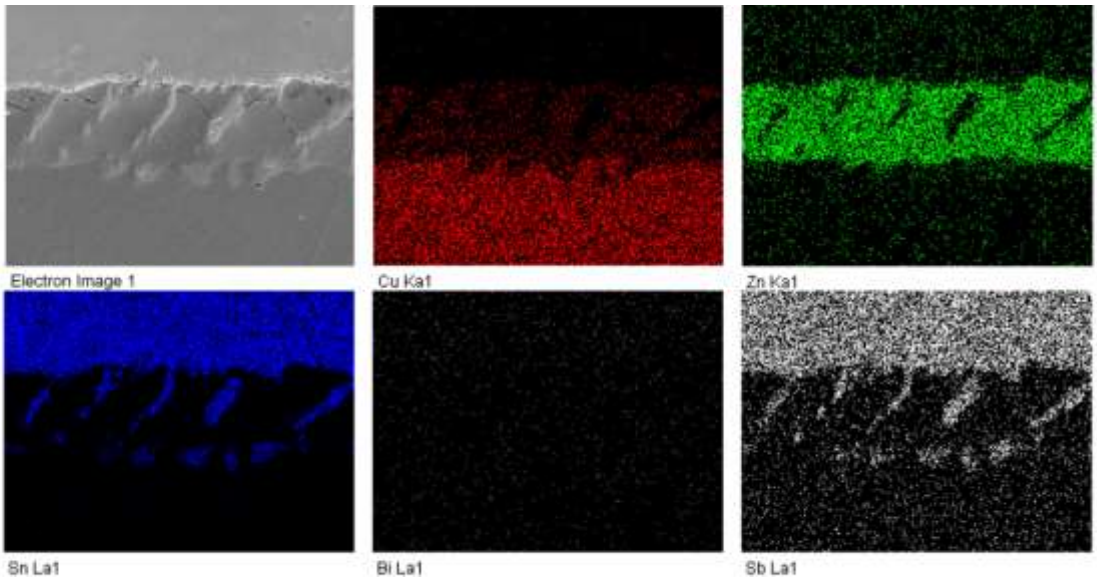

Figure 9 SEM morphology and EPMA mapping analysis of Sn-8Zn-3Bi-1.5Sb/Cu interface after aging of 720 h

Figure 10 shows the schematic diagram presenting thermodynamic interfacial reaction of Sn-8Zn-3Bi-xSb/Cu during reflowing and aging, and is elucidated as follows:

b) When the melting Sn-8Zn-3Bi-xSb solder alloy contacts the Cu substrate, Zn atoms from the solder bulk and Cu atoms from the substrate diffuse towards the interface and form γ-Cu_5-Zn_8.

c) During soldering, ε-$CuZn_5$ is formed through two subsequent peritectic reactions, i.e., L + γ-Cu_5Zn_8 → δ-$CuZn_3$ and L + γ-$CuZn_3$ → ε-$CuZn_5$.

d) Due to Cu's higher diffusivity than Zn, upon initial aging, newly formed ε-$CuZn_5$ is converted to γ-Cu_5Zn_8. Some Cu atoms diffuse and penetrate the IML, to form γ-Cu_5Zn_8 with the Zn phase within the solder bulk.

e) The depletion of Zn leads to the degradation of unstable Cu_5Zn_8, thus initialling forming voids within the IML and which are subsequently filled rapidly by diffusing Sn atoms.

f) These Sn atoms from the solder alloy tunnel to the Cu substrate and form Cu_6Sn_5.

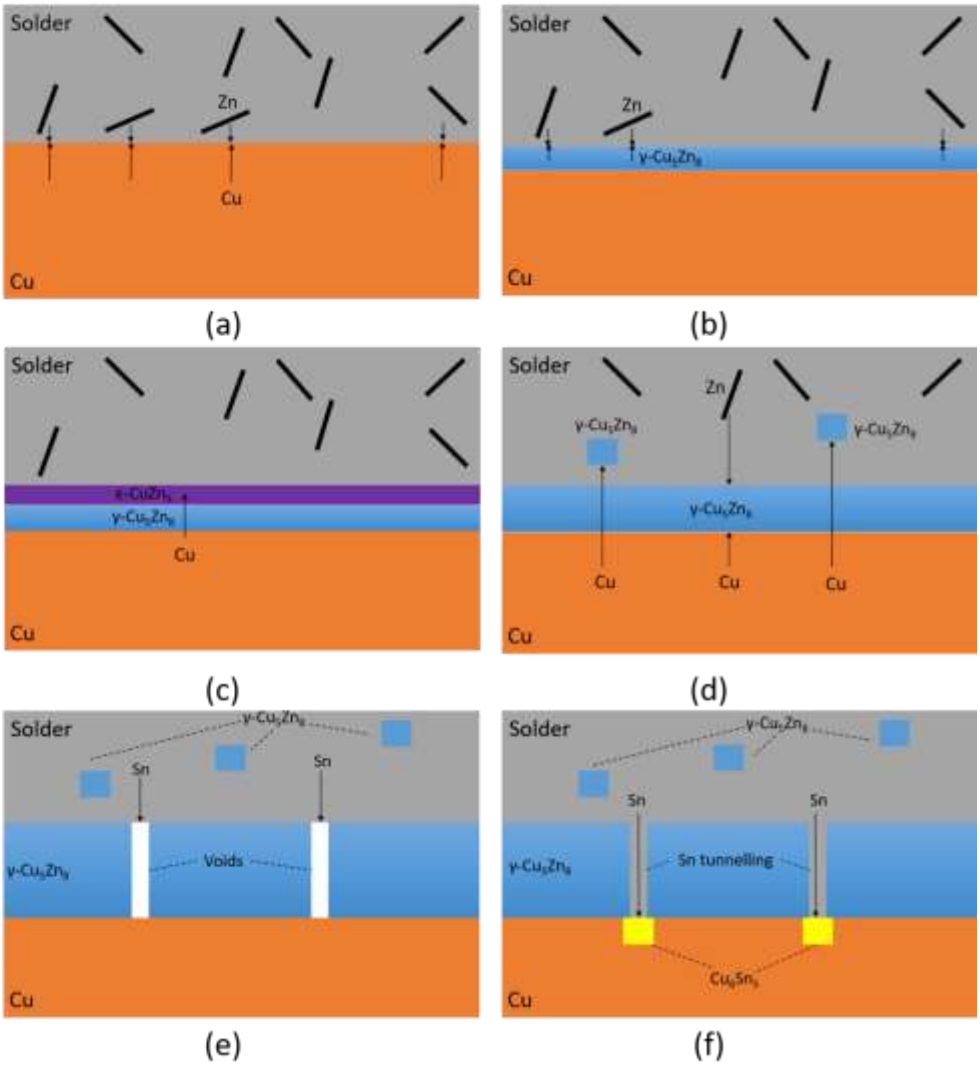

Figure 10 Schematic diagram to indicate thermodynamic interfacial reaction during reflowing: (a) the diffusion of Zn and Cu, (b) formation of γ-Cu_5Zn_8 IML and (c) formation of ε-$CuZn_5$ IML; and during aging: (d) transformation of ε-$CuZn_5$ to γ-Cu_5Zn_8 IML and formation of γ-Cu_5Zn_8 particles within solder matrix; (e) depletion of Zn and emergence of voids; (f) Sn tunnelling and formation of Cu_6Sn_5

Figure 11 shows that the average thickness of γ-Cu_5Zn_8 IML in all joint coupons increases as the aging time increases, and this growth follows the square root time law. This indicates that the IML growth of Sn-8Zn-3Bi-xSb/Cu interface is mainly controlled by diffusion of elements to the reaction interface.

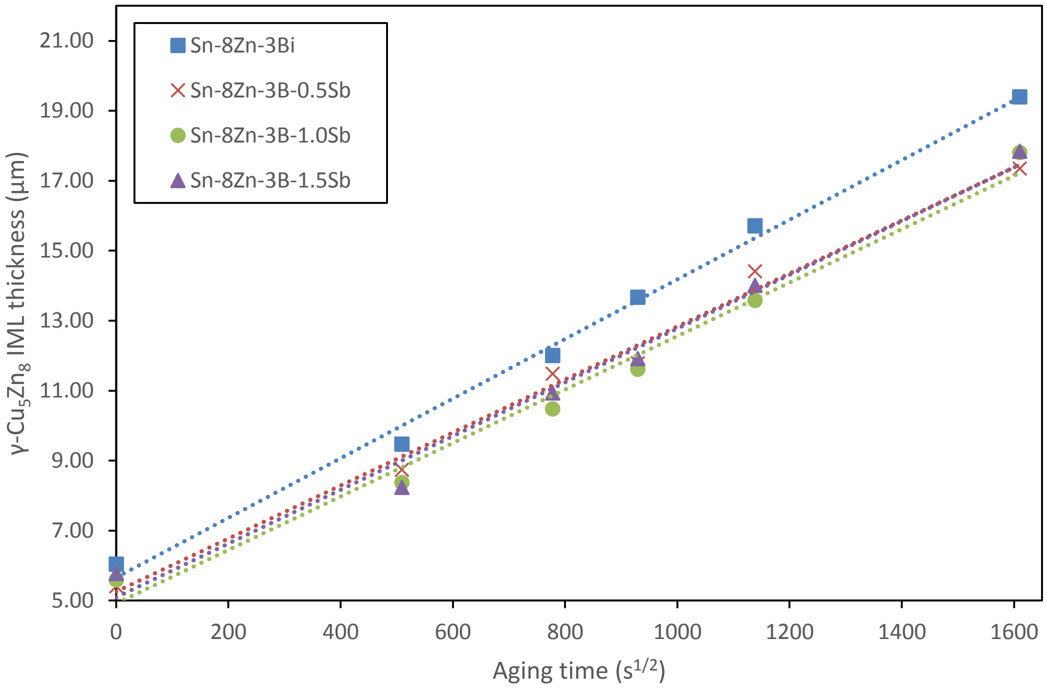

Figure 11 Thickness of IML with different aging time at the interface between Sn-8Zn-3Bi-xSb solder alloys and Cu substrate.

The change of IML thickness as a function of time can be fitted to Fick's law:

$$d - d_0 = (kt)^{1/2}$$

where d is the thickness of the IMC layer, d_0 is the initial thickness, k is the growth rate constant, and t is the growing time.

The growth rate constant $k^{1/2}$ of each solder couple is listed in Table 2. It can be found that Sb alloyed solder coupons show marginally slower growth rate, which presumably indicates that Sb retarded the IML thickening at Sn-8Zn-3Bi-xSb/Cu interface.

Table 2 The slope (growth rate constant $k^{1/2}$) of IML thickness

	Slope $k^{1/2}$	Linearity R^2
Sn-8Zn-3Bi	0.0085	0.9943
Sn-8Zn-3B-0.5Sb	0.0076	0.9905
Sn-8Zn-3B-1.0Sb	0.0076	0.9853
Sn-8Zn-3B-1.5Sb	0.0077	0.9851

Sb is detected in not only Sn matrix of solder bulk but also Sn tunnels, as revealed in Figure 9, which indicates the high solubility of Sb in Sn. As discussed above, IML thickening is mainly controlled by diffusion of elements, it can be hypotheses that Sb micro alloy has the pinning effect therefore to reduce the diffusion rate of Zn in Sn matrix, eventually supressing the growth of Cu_5Zn_8 IML.

Conclusions

The interfacial reaction at the interface of Sn-8Zn-3Bi-xSb/Cu in soldering and the interfacial evolution during isothermal aging has been studied. An interfacial reaction mechanism has been proposed and summarised as follows: Cu_5Zn_8 and $CuZn_5$ IMLs were initially formed at the Sn-8Zn-3Bi-xSb/Cu interface after soldering, however $CuZn_5$ was transformed to Cu_5Zn_8 upon initial aging. While Cu_5Zn_8 was the dominant reaction product at the interface, it is unstable and can degrade once Zn is depleted, gradually forming a number of voids throughout the IML. Sn atoms rapidly fill up these voids and tunnel to the Cu substrate and to form Cu_5Sn_6 at the IML/Cu interface. The addition of Sb did not alter this reaction mechanism or introduce any new IMCs, but supresses the IML thickening at the interface. Hypothetically, Sb micro-alloys homogeneously dissolved in Sn reduced the diffusion rate of Zn in Sn matrix though the pinning effect.

Acknowledgment

This work has been funded by the Irish Research Council in partnership with Henkel Ltd under the Enterprise Partnership Scheme grant number EPSG/2014/48.

Data availability statement

The raw/processed data required to reproduce these findings cannot be shared at this time as the data also forms part of an ongoing study.

References

[1] G. Henshall, R. Healey, R. S. Pandher, K. Sweatman, K. Howell, R. Coyle*, et al.*, "iNEMI Pb-free alloy alternatives project report: state of the industry," in *Proceedings SMTA International*, 2008.

[2] D. Shangguan, *Lead-free solder interconnect reliability*: ASM international, 2005.

[3] H. Ma and J. C. Suhling, "A review of mechanical properties of lead-free solders for electronic packaging," *Journal of Materials Science,* vol. 44, pp. 1141-1158, Mar 2009.

[4] R. Coyle, M. Reid, C. Ryan, R. Popowich, P. Read, D. Fleming*, et al.*, "The influence of the Pb-free solder alloy composition and processing parameters on thermal fatigue performance of a ceramic chip resistor," in *Electronic Components and Technology Conference, 2009. ECTC 2009. 59th*, 2009, pp. 423-430.

[5] D. A. Shnawah, M. F. M. Sabri, and I. A. Badruddin, "A review on thermal cycling and drop impact reliability of SAC solder joint in portable electronic products," *Microelectronics Reliability,* vol. 52, pp. 90-99, 1// 2012.

[6] F. J. Cheng, F. Gao, J. Y. Zhang, W. S. Jin, and X. Xiao, "Tensile properties and wettability of SAC0307 and SAC105 low Ag lead-free solder alloys," *Journal of Materials Science,* vol. 46, pp. 3424-3429, May 2011.

[7] M. Reid, J. Punch, M. Collins, and C. Ryan, "Effect of Ag content on the microstructure of Sn-Ag-Cu based solder alloys," *Soldering & Surface Mount Technology,* vol. 20, pp. 3-8, 2008.

[8] M. N. Collins, E. Dalton, and J. Punch, "Microstructural influences on thermomechanical fatigue behaviour of third generation high Ag content Pb-Free solder alloys," *Journal of Alloys and Compounds,* vol. 688, pp. 164-170, Dec 15 2016.

[9] K. S. Kim, S. H. Huh, and K. Suganuma, "Effects of intermetallic compounds on properties of Sn-Ag-Cu lead-free soldered joints," *Journal of Alloys and Compounds,* vol. 352, pp. 226-236, Mar 24 2003.

[10] E. Dalton, G. Ren, J. Punch, and M. N. Collins, "Accelerated temperature cycling induced strain and failure behaviour for BGA assemblies of third generation high Ag content Pb-free solder alloys," *Materials & Design,* vol. 154, pp. 184-191, Sep 15 2018.

[11] M. N. Collins, J. Punch, and R. Coyle, "Surface finish effect on reliability of SAC 305 soldered chip resistors," *Soldering & Surface Mount Technology,* vol. 24, pp. 240-248, 2012.

[12] R. A. Islam, Y. C. Chan, W. Jillek, and S. Islam, "Comparative study of wetting behavior and mechanical properties (microhardness) of Sn-Zn and Sn-Pb solders," *Microelectronics Journal,* vol. 37, pp. 705-713, Aug 2006.

[13] S. Liu, S. B. Xue, P. Xue, and D. X. Luo, "Present status of Sn-Zn lead-free solders bearing alloying elements," *Journal of Materials Science-Materials in Electronics,* vol. 26, pp. 4389-4411, Jul 2015.

[14] G. J. Jackson, I. J. Wilding, R. Boyle, M. N. Collins, E. Dalton, J. Punch*, et al.*, "SnZn Solder Alternative For Low-Cost Pb-Free Surface Mount Assemblies," in *SMTA International*, 2012.

[15] L. Zhang, J. H. Cui, J. G. Han, Y. H. Guo, and C. W. He, "Microstructures and properties of SnZn-xEr lead-free solders," *Journal of Rare Earths,* vol. 30, pp. 790-793, Aug 2012.

[16] C. M. L. Wu, C. M. T. Law, D. Q. Yu, and L. Wang, "The wettability and microstructure of Sn-Zn-RE alloys," *Journal of Electronic Materials,* vol. 32, pp. 63-69, Feb 2003.

[17] J. Q. Huang, M. B. Zhou, C. Z. Li, X. Ma, and X. P. Zhang, "Processing Performance and Microstructure of Sn-Zn Based Solders Modified by Bi and Mixed Rare Earth Elements," *2012 13th International Conference on Electronic Packaging Technology & High Density Packaging (Icept-Hdp 2012),* pp. 351-354, 2012.

[18] Y. Sun, F. Xue, and J. Zhou, "Lead-free solders based on the Sn-8Zn-3Bi ternary alloy with additions of In, Nd or La," in *Electronic Packaging Technology, 2005 6th International Conference on*, pp. 253-257.

[19] H. Ye, S. B. Xue, J. D. Luo, and Y. Li, "Properties and interfacial microstructure of Sn-Zn-Ga solder joint with rare earth Pr addition," *Materials & Design,* vol. 46, pp. 816-823, Apr 2013.

[20] A. A. El-Daly, A. E. Hammad, G. A. Al-Ganainy, and A. A. Ibrahiem, "Enhancing mechanical response of hypoeutectic Sn-6.5Zn solder alloy using Ni and Sb additions," *Materials & Design,* vol. 52, pp. 966-973, Dec 2013.

[21] A. A. El-Daly, A. E. Hammad, G. S. Al-Ganainy, and A. A. Ibrahiem, "Design of lead-free candidate alloys for low-temperature soldering applications based on the hypoeutectic Sn-6.5Zn alloy," *Materials & Design,* vol. 56, pp. 594-603, Apr 2014.

[22] K. Suganuma, K. Niihara, T. Shoutoku, and Y. Nakamura, "Wetting and interface microstructure between Sn-Zn binary alloys and Cu," *Journal of Materials Research,* vol. 13, pp. 2859-2865, Oct 1998.

[23] G. Ren, I. J. Wilding, and M. N. Collins, "Alloying influences on low melt temperature SnZn and SnBi solder alloys for electronic interconnections," *Journal of Alloys and Compounds,* vol. 665, pp. 251-260, Apr 25 2016.

[24] K. Suganuma and K. S. Kim, "Sn-Zn low temperature solder," *Journal of Materials Science-Materials in Electronics,* vol. 18, pp. 121-127, Mar 2007.

[25] Y. H. Ko, J. D. Lee, T. Yoon, C. W. Lee, and T. S. Kim, "Controlling Interfacial Reactions and Intermetallic Compound Growth at the Interface of a Lead-free Solder Joint with Layer-by-Layer Transferred Graphene," *Acs Applied Materials & Interfaces,* vol. 8, pp. 5679-5686, Mar 2 2016.

[26] L. Liu, P. Wu, and W. Zhou, "Effects of Cu on the interfacial reactions between Sn-8Zn-3Bi-xCu solders and Cu substrate," *Microelectronics Reliability,* vol. 54, pp. 259-264, Jan 2014.

[27] L. J. Liu, W. Zhou, B. L. Li, and P. Wu, "Interfacial reactions between Sn-8Zn-3Bi-xAg lead-free solders and Cu substrate," *Journal of Alloys and Compounds,* vol. 482, pp. 90-98, Aug 12 2009.

[28] C. M. Chen and C. H. Chen, "Interfacial reactions between eutectic SnZn solder and bulk or thin-film cu substrates," *Journal of Electronic Materials,* vol. 36, pp. 1363-1371, Oct 2007.

[29] C. W. Huang and K. L. Lin, "Interfacial reactions of lead-free Sn-Zn based solders on Cu and Cu plated electroless Ni-P/Au layer under aging at 150 degrees C," *Journal of Materials Research,* vol. 19, pp. 3560-3568, Dec 2004.

[30] C. T. Lin, C. S. Hsi, M. C. Wang, T. C. Chang, and M. K. Liang, "Interfacial microstructures and solder joint strengths of the Sn-8Zn-3Bi and Sn-9Zn-lAl Pb-free solder pastes on OSP finished printed circuit boards," *Journal of Alloys and Compounds,* vol. 459, pp. 225-231, Jul 14 2008.

[31] L. L. Duan, D. Q. Yu, S. Q. Han, H. T. Ma, and L. Wang, "Microstructural evolution of Sn-9Zn-3Bi solder/Cu joint during long-term aging at 170 degrees C," *Journal of Alloys and Compounds,* vol. 381, pp. 202-207, Nov 3 2004.

[32] G. Ren and M. N. Collins, "The effects of antimony additions on microstructures, thermal and mechanical properties of Sn-8Zn-3Bi alloys," *Materials & Design,* vol. 119, pp. 133-140, 2017.

[33] H. M. Lee, S. W. Yoon, and B.-J. Lee, "Thermodynamic prediction of interface phases at Cu/solder joints," *Journal of electronic materials,* vol. 27, pp. 1161-1166, 1998.

[34] C. Y. Chou and S. W. Chen, "Phase equilibria of the Sn-Zn-Cu ternary system," *Acta Materialia,* vol. 54, pp. 2393-2400, May 2006.

[35] J. S. Kirkaldy and D. J. Young, *Diffusion in the condensed state*: Institute of metals London, 1987.

[36] K. N. Tu and K. Zeng, "Tin-lead (SnPb) solder reaction in flip chip technology," *Materials Science & Engineering R-Reports,* vol. 34, pp. 1-58, Jul 2 2001.

[37] T. B. Massalski, H. Okamoto, P. Subramanian, and L. Kacprzak, "Binary alloy phase diagrams. vol. 3," *ASM International, 1990,* p. 1485, 1990.

[38] R. Hultgren, P. D. Desai, D. T. Hawkins, M. Gleiser, and K. K. Kelley, "Selected values of the thermodynamic properties of binary alloys," National Standard Reference Data System1973.

[39] M. Date, K. N. Tu, T. Shoji, M. Fujiyoshi, and K. Sato, "Interfacial reactions and impact reliability of Sn-Zn solder joints on Cu or electroless Au/Ni(P) bond-pads," *Journal of Materials Research,* vol. 19, pp. 2887-2896, Oct 2004.

[40] R. Mayappan, A. B. Ismail, Z. A. Ahmad, T. Ariga, and L. B. Hussain, "The effect of crosshead speed on the joint strength between Sn-Zn-Bi lead-free solders and Cu substrate," *Journal of Alloys and Compounds,* vol. 436, pp. 112-117, Jun 14 2007.

[41] S. W. Chen, C. M. Chen, and W. C. Liu, "Electric current effects upon the Sn/Cu and Sn/Ni interfacial reactions," *Journal of Electronic Materials,* vol. 27, pp. 1193-1198, Nov 1998.

[42] R. R. Hultgren, *Selected values of thermodynamic properties of metals and alloys*: John Wiley & Sons Inc, 1963.

[43] K. Suganuma, T. Murata, H. Noguchi, and Y. Toyoda, "Heat resistance of Sn–9Zn solder/Cu interface with or without coating," *Journal of Materials Research,* vol. 15, pp. 884-891, 2000.